CT-1042, a novel anticancer agent, exhibits effects by activating p53 and inhibiting survivin

JUN YANG[1,2], LINNA LI[2], CHENGWANG XU[2], DEXUAN YANG[2], SHANSHAN WANG[2] and SHOUJUN YUAN[1,2]

[1]School of Graduate Studies, Anhui Medical University, Hefei, Anhui 230032;
[2]Beijing Institute of Radiation Medicine, Beijing 100850, P.R. China

Abstract. A novel small molecular compound, 4-ethyl-8-fluoro-hydroxy-9-methoxy-11-methyl-1,12-dihydro-4H-2-oxa-6,12a-diaza-dibenzo[b,h]fluorene-3,13-dione (CT-1042) exhibits potent antitumor activity against many tumor cells *in vitro*. However, the effects and underlying mechanisms of CT-1042 in non-small cell lung cancer (NSCLC) remain unclear. The present study was designed to determine the anticancer properties and underlying molecular mechanisms of CT-1042 in NCI-H460 NSCLC cells. A thiazolyl blue tetrazolium bromide assay (MTT) was performed to evaluate cell viability and flow cytometry was used to analyze apoptosis, mitochondrial membrane potential (MMP) and cell cycle. Real-time quantitative PCR and western blotting were conducted to determine relative mRNA and protein levels. A tumor xenograft experiment was performed to investigate the effects of CT-1042 on tumor growth *in vivo*. CT-1042 markedly inhibited the proliferation of twelve cancer cell lines, decreased MMP in subject cells and increased caspase-3 activity. Cell cycle analysis indicated that CT-1042 delayed the cell cycle progression during the G2/M phase in a dose-dependent manner. In addition, CT-1042 induced mitochondrial-mediated apoptosis by activating p53 and Bax, as well as inhibiting Bcl-2 and survivin. Finally, CT-1042 significantly suppressed NCI-H460 xenograft tumor growth *in vivo*, with low systemic toxicity. Collectively, these results revealed that CT-1042 has significant lung anticancer properties.

Correspondence to: Professor Shoujun Yuan, Beijing Institute of Radiation Medicine, 27 Taiping Road, Haidian, Beijing 100850, P.R. China
E-mail: yuansj@nic.bmi.ac.cn

Introduction

Malignant tumors are difficult to treat and represent a major health problem worldwide. Camptothecin is an anticancer drug that is derived from the bark of the Chinese tree *Camptotheca accuminata* and has demonstrated significant antitumor activity (1,2). However, its use is limited due to severe and unpredictable adverse effects such as myelosuppression, vomiting, diarrhea and severe hemorrhagic cystic disease (3). Structural modification of camptothecin resulted in CT-1042 (Fig. 1A and B), a novel compound with very low toxicity that activates the tumor suppressor p53 and inhibits survivin (an inhibitor of apoptosis).

In recent years, rapid developments in the field of medicine have resulted in target-specific antitumor agents with high selectivity for tumor cells and low toxicity in normal cells, including targeted tyrosine kinases (4-6), angiogenesis (7,8), tumor cell cycle-related factors, histone deacetylase, tumor microenvironment and tumor stem cells (9). Lung cancer pathogenesis is related to the expression of key signaling proteins, as well as phosphorylation and dephosphorylation events that can lead to abnormal cell proliferation and survival (10). Among tumor suppressors, p53 and the caspase-family proteins play key roles in cancer development and apoptosis (11). Numerous p53 activators have been identified or used in clinical trials, including JNJ-26854165 (12) and XI-011 (13).

The *p53* gene codes for a protein that regulates the cell cycle and functions as a tumor suppressor (14). The p53 protein is activated in response to different types of cellular stress signals, such as DNA damage and oncogene activation, which induce several protective responses, including cell cycle arrest, aging or cell apoptosis (15,16). The mitochondrial pathway and the death receptor pathway both induce apoptosis. However, the mitochondrial pathway is related to multiple factors such as the Bcl-2 family of proteins, cytochrome *c* (CYCS) and caspases (17,18). Activation of p53 triggers an increase in the expression of the Bcl-2-family protein Bax, which targets the mitochondria and induces CYCS release, followed by activation of caspase-9 and the intrinsic apoptosis pathway (19).

CT-1042 ($C_{22}H_{19}O_5N_2F$) was provided by Chifeng Saliont Pharmaceutical Co., Ltd. (Chifeng, China). In the present study, we investigated the anticancer effects of CT-1042 *in vitro* and *in vivo* and explored the underlying mechanisms

for CT-1042-mediated apoptosis in NCI-H460 cells in order to provide an experimental basis for its drug properties.

Materials and methods

Chemicals and antibodies. CT-1042 injections and additional solvent were provided by Chifeng Saliont Pharmaceutical Co., Ltd., and were stored at 4˚C. Thiazolyl blue tetrazolium bromide (MTT) was purchased from Beijing Jingkehongda Biotechnology Co., Ltd., (Beijing, China). The Annexin V-fluorescein isothiocyanate/propidium iodide (FITC/PI) Apoptosis kit, mitochondrial membrane potential assay kit with JC-1, caspase-3 activity assay kit, and Hoechst 33342 were purchased from BestBio (Shanghai, China). TRIzol reagent, HiFiScript gDNA Removal cDNA Synthesis kit, UltraSYBR mixture and enhanced chemiluminescence (ECL) detection kit were purchased from CWBIO (Beijing, China). All primers were synthesized by Invitrogen (Shanghai, China).

Anti-β-actin antibody (1:1,000; cat. no. 01264), goat anti-rabbit secondary antibody (1:2,000; 1:100; cat. no. CW0103S) and goat anti-mouse secondary antibody (1:2,000, 1:100; cat. no. CW0102S) were purchased from CWBIO. The anti-Bcl-2 (1:1,000; cat. no. 2870P), anti-Bax (1:1,000; cat. no. 2772S), anti-caspase-3 (1:250; cat. no. 9664S), anti-c-met (1:1,000; cat. no. 4560S) and anti-c-myc (1:1,000; cat. no. 9402S) antibodies were purchased from Cell Signaling Technology (Danvers, MA, USA). The anti-p53 (1:1,000; cat. no. ab26), anti-Apaf-1 (1:1,000, cat. no. ab32372), anti-caspase-9 (1:2,000; cat. no. ab202068), anti-Ki-67 (1:200; cat. no. ab16667), anti-survivin (1:5,000; 1:250; cat. no. ab76424) and anti-poly ADP-ribose polymerase-1 (PARP) (1:2,000; cat. no. ab32138) antibodies were purchased from Abcam (Cambridge, UK). The anti-CYCS (1:1,000; cat. no. A0225) and anti-STAT1 (1:1,000; cat. no. A10100) antibodies were purchased from ABclonal (Wuhan, China).

Cell culture. The human lung cancer cell lines NCI-H460 and NCI-H446, the human breast cancer cell lines MCF-7 and MDA-MB-231, the human kidney cancer cell line KCC-853 (20), the human liver cancer cell lines MHCC97H and HCCLM3, the human colon cancer cell lines HCT-116 and LoVo, the human prostate cancer cell line T24, the human gastric cancer cell line SGC-7901 and the human leukemia cell line K-562 were obtained from the National Infrastructure of Cell Line Resource (Beijing, China). Cell lines were regularly checked for identity, including mycoplasma tests. All cells were cultured in RPMI-1640 medium (Thermo Fisher Scientific, Shanghai, China) or Dulbecco's modified Eagle's medium (DMEM; Thermo Fisher Scientific), supplemented with 10% fetal bovine serum (FBS; Yuanhengshengma Biotechnology, Co., Ltd., Beijing, China) and 1% penicillin- streptomycin and incubated in 5% CO_2 at 37˚C. Cell medium was changed every two days.

MTT assay. CT-1042 cytotoxicity was determined by an MTT assay. Different tumor cell lines that were exponentially growing were seeded onto 96-well plates with 2,000-4,000 cells/well. After culturing overnight, the cells were treated with CT-1042 at a range of concentrations for

72 h. MTT solution (0.5 mg/ml) was then added to each well and the 96-well plates were further incubated for 4 h at 37˚C. To dissolve the formazan crystals formed by viable cells, 200 μl dimethyl sulfoxide (DMSO) was added to each well and absorbance at 570 nm was assessed using a microplate reader (SPECTROstarNano; BMG Labtech, Ortenberg, Germany).

Hoechst 33342 staining. Cells were seeded in 6-well plates at $2x10^5$ cells/well and treated with 0, 0.15, 0.6 or 2.4 nmol/l CT-1042 for 24 h. The cells were fixed with 4% paraformaldehyde for 20 min and then stained with Hoechst 33342 (3 μg/ml) for 10 min. After washing with phosphate-buffered saline (PBS), morphological changes in the cells were observed under a fluorescent microscope (Etaluma, Inc., Carlsbad, CA, USA).

Annexin V/PI staining assay. Lung cancer cells were treated with CT-1042 for 24 h and then cells were harvested using centrifugation. Apoptosis was quantified with an Annexin V-FITC/PI kit according to the manufacturer's protocol. Cells were stained with Annexin V (1 μl) and PI (2 μl) for 20 min at room temperature, in the dark. For each sample, 5,000 cells were collected and flow cytometry (FCM) was employed to analyze cellular apoptosis (guavaSoft software version 2.7; Merck Millipore, Darmstadt, Germany).

Mitochondrial membrane potential (MMP). Decreased MMP is a landmark event during cellular apoptosis. Collected cells were suspended in pre-configured JC-1 staining solution (500 μl) according to the MMP assay kit instructions. After incubating for 15 min at 37˚C, cells were centrifuged and then resuspended in the preheated incubation buffer. FCM analysis was performed immediately to detect decreases in MMP.

Cell cycle analysis. Cells collected in the previous step were suspended in 500 μl PBS and mixed with 500 μl absolute ethanol. After 1 h at 4˚C, cells were resuspended in 800 μl PBS containing 10 μl RNase (10 mg/ml) for 30 min at 37˚C, and then 500 μl of PBS containing 25 μl PI (1 mg/ml) for 5 min in the dark. Nuclear DNA content was analyzed using FCM. Data analysis was performed using ModFit software (Verity Software House Inc., Topsham, ME, USA).

Caspase-3 activity. Caspase-3 protease activity was assessed according to the caspase-3 activity assay kit protocol. In brief, the same number of cells ($2-5x10^6$) was collected for each sample and lysed. Protein lysates (10 μl) and Ac-DEVD-pNA (10 μl) were then added to the detection buffer (90 μl) for 120 min at 37˚C; each sample was added to 3 parallel wells. Absorbance (405 nm) was assessed with a microplate reader (SPECTROstarNano; BMG Labtech) and the relative activity (RA) was calculated.

Real-time quantitative PCR (RT-qPCR). Total cellular RNA was isolated using TRIzol reagent (CWBIO). A HiFiScript gDNA removal cDNA synthesis kit was used to remove the gDNA and synthesize the cDNA. The cDNA was then subjected to RT-qPCR to quantify the relative transcript levels using the UltraSYBR mixture according to the manufacturer's instructions. Reaction conditions included 1 cycle of 95˚C for

Table I. Primer sequences used in RT-qPCR.

No.	Gene	Forward primer	Reverse primer
1	β-actin	GAAGATCAAGATCATTGCTCCTC	ATCCACATCTGCTGGAAGG
2	P53	CTCAGATAGCGATGGTCTGG	CTGTCATCCAAATACTCCACAC
3	Bax	TAACATGGAGCTGCAGAGG	CAGTTGAAGTTGCCGTCAG
4	Bik	CTTTGGAATGCATGGAGGG	AGATGAAAGCCAGACCCAG
5	Apaf-1	GAAATGAGCCCACTCAACAG	GAGCATTGTAGAATGATACGTAGG
6	Caspase-9	AAACCAGAGGTTCTCAGACC	AACTCTCAAGAGCACCGAC
7	Survivin	CTGGACAGAGAAAGAGCCA	CTTTCTCCGCAGTTTCCTC

10 min, followed by 45 cycles of 95˚C for 10 sec and 60˚C for 30 sec. A melting curve was determined at 95˚C for 1 min, 55˚C for 30 sec and 95˚C for 30 sec. Data were analyzed with the $\Delta\Delta Cq$ method (21). The primer sequences used for the present study are listed in Table I.

Western blotting. Treated and untreated cells were washed twice with cold PBS and lysed for 30 min with radioimmunoprecipitation assay (RIPA) lysis buffer containing protease inhibitor cocktail and phosphatase inhibitor cocktail. Cell lysates were centrifuged at 13,523 x g for 20 min at 4˚C. Total protein concentrations were determined with the bicinchoninic acid (BCA) protein assay kit. Equal amounts of protein (50 μg) from each group were separated by different concentrations of sodium dodecyl sulfate polyacrylamide gel electrophoresis (SDS-PAGE) and transferred onto polyvinylidene difluoride (PVDF) membranes (Millipore, Billerica, MA, USA). Membranes were blocked with 5% non-fat milk in Tris-buffered saline with Tween-20 (TBS-T) for 1 h at room temperature, blotted overnight at 4˚C with specific primary antibodies, washed three times with TBS-T, and then probed with the corresponding horseradish peroxidase (HRP)-linked secondary antibodies for 1 h at room temperature. Finally, an ECL detection kit was applied to assess the immunoreactive signals, and the software used for western blot analysis was Chemi Capture (Shanghai Clinx Science Instruments Co., Ltd., Shanghai, China).

In vivo tumor xenograft experiments. Nu/Nu female nude mice with body masses ranging from 20 to 22 g were purchased from Beijing Vital River Laboratory Animal Technology Co., Ltd. (Beijing, China). The experiment was performed in accordance with the principles of antitumor pharmacodynamics and the standard protocols established by the Ethics Committee of the Academy of Military Medical Sciences. Three nude mice were inoculated with NCI-H460 cells [1×10^7 cells/mouse, subcutaneously (s.c.)]. Once the tumors reached a volume of ~1,500-2,000 mm³, they were removed under sterile conditions and cut into pieces of ~1.0x1.0x1.0 mm³ and then inoculated subcutaneously in the right flank of all mice (n=45). When tumors reached 100 mm³, five mice were eliminated (tumor volume is too large or too small), and the remaining mice were randomized into five groups (n=8) including control, paclitaxel [15 mg/kg, intravenously (i.v.), three times per week], high-dose (0.1 mg/kg, i.v., weekly), middle-dose (0.05 mg/kg, i.v., weekly)

and low-dose (0.025 mg/kg, i.v., weekly). Mice were treated for 15 days and then sacrificed (euthanasia, 100% CO_2). Partial xenograft tumors were used for hematoxylin and eosin (H&E) staining and immunohistochemistry (IHC) analyses. Tumor sizes were assessed every 2 days using Vernier calipers and the tumor volume (V) was calculated using the following formula: $V = (\text{length x width}^2) \times \frac{1}{2}$; the evaluation index included the inhibition rate of tumor volume and the inhibition rate of tumor weight.

H&E staining and immunohistochemistry analysis. The separated tumor tissues were fixed with 4% formalin for 48 h and embedded in paraffin. The tissue sections (4 μm thick) were prepared and stained with H&E for tissue pathology and then observed under a microscope (Advanced Microscopy Group, Bothel, WA, USA). For IHC analysis, in brief, the tissue sections were deparaffinized, rehydrated and endogenous peroxidase activity-blocked with 3% hydrogen peroxide at room temperature. Antigen retrieval using citrate buffer and a microwave technique was then performed, along with blocking of non-specific binding sites. Subsequently, the primary antibodies (anti-Ki-67, anti-survivin and anti-caspase-3) were applied overnight, followed by the homologous secondary antibodies. In general, 3,3'-diaminobenzidine (DAB) staining, slight hematoxylin staining and neutral balata fixation were applied.

Statistical analysis. Origin 8.5 software (OriginLab, Northampton, MA, USA) and GraphPad Prism 5 (GraphPad Software, Inc., La Jolla, CA, USA) software were used to process the data. The results are presented as the means ± standard deviation (SD). A one-way analysis of variance (ANOVA, Tukey method) was used to assess significant differences among experimental groups. $P<0.05$ was considered to indicate a statistically significant difference.

Results

CT-1042 suppresses the proliferation of different tumor cells. We assessed the influence of CT-1042 on the growth of different tumor cells using an MTT assay. Experimental results demonstrated that CT-1042 had a marked inhibitory effect on most of the tumor cells tested (Table II). Particularly, the half-maximal inhibitory concentration (IC_{50}) after incubation for 72 h was 0.166±0.004 nmol/l in NCI-H460 cells, demonstrating a

Table II. Effect of CT-1042 on different tumor cells *in vitro* (IC_{50}, nmol/l).

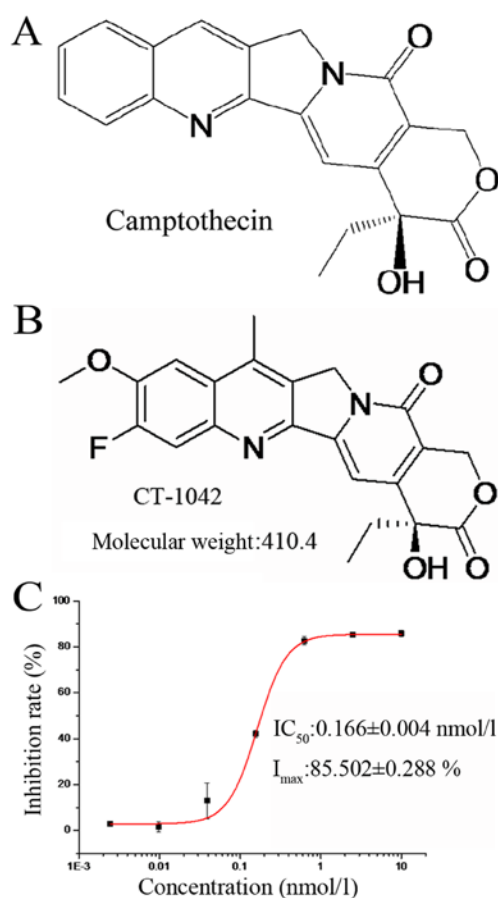| No.	Cell lines	First time	Second time
1	NCI-H460	0.17±0.01	0.15±0.024
2	NCI-H446	52.86±11.63	34.93±6.93
3	MCF-7	1.14±1.04	0.14±0.12
4	MDA-MB-231	3.40±0.90	4.16±1.24
5	KCC-853	143.13±37.59	97.77±57.59
6	MHCC97H	89.64±24.85	74.63±20.79
7	HCCLM3	1.25±0.05	1.23±0.05
8	HCT-116	1.36±0.24	1.12±0.30
9	LoVo	190.73±31.53	172.02±38.75
10	T24	0.38±0.05	0.41±0.05
11	SGC-7901	0.94±0.06	1.02±0.04
12	K562	0.17±0.02	0.17±0.03

Figure 1. CT-1042 suppresses NCI-H460 cell proliferation. (A) The chemical structure of camptothecin. (B) The chemical structure and molecular weight of CT-1042. (C) NCI-H460 cells were treated with different concentrations of CT-1042 for 72 h and the inhibition rate was tested via the thiazolyl blue tetrazolium bromide (MTT) assay.

dose-dependent effect (Fig. 1C). Therefore, we used the human lung cancer NCI-H460 cell line in the subsequent experiments to explore the specific mechanisms.

CT-1042 induces NCI-H460 cellular apoptosis. The Annexin V-FITC/PI assay was used to evaluate the effects of CT-1042 on apoptosis. As demonstrated, a dose-dependent increase in the proportion of apoptotic cells (early and late) was observed, which was significantly higher than that observed in the control group (Fig. 2A and E). Furthermore, Hoechst 33342 staining revealed a gradual decrease in the number of cells with increasing concentrations of CT-1042; chromatin shrinkage and nuclear fragmentation increased, as shown by the red arrows (Fig. 2C). The JC-1 fluorescent probe indicated disruption of MMP, which is one of the earliest apoptotic events (22) (Fig. 2B). Finally, CT-1042 (2.4 nM) increased caspase-3 activity three-fold, as determined using the caspase-3 activity assay (Fig. 2D).

CT-1042 induces G2/M cell cycle arrest in NCI-H460 cells. Cell cycle distribution was analyzed with PI staining and FCM. The expected cell cycle pattern for continuously growing cells was observed in the control cells, whereas CT-1042-treated cells displayed a dose-dependent and progressive accumulation in the G2/M phase accompanied by a decrease in the number of cells in the G0/G1 phase (Fig. 3). This finding indicated that CT-1042 significantly induced G2/M cycle arrest in NCI-H460 cells, which may be a mechanism contributing to cellular apoptosis.

CT-1042-induced regulation of mRNA expression in NCI-H460 cells. The mitochondrial apoptotic pathway is one of the main apoptotic pathways. Bcl-2 family regulates apoptosis by controlling mitochondrial permeability and the release of CYCS. To explore the effects of CT-1042 on mRNA expression in NCI-H460 cells, we examined the mitochondrial apoptotic pathway, including the expression of *p53*, *Bax*, *Bik*, *Apaf-1*, *Casp9* and *survivin* using RT-qPCR analyses. As displayed in Fig. 4A, CT-1042 significantly upregulated the expression of *p53*, *Bax*, *Bik*, *Apaf-1* and *Casp9*, and downregulated the expression of *survivin*, indicating that CT-1042 further promoted the downstream caspase cascade by activating p53 and inhibiting survivin.

Effects of CT-1042 on the activation of p53 and mitochondria-mediated apoptosis in NCI-H460 cells. Detectable p53 mRNA was easily determined in NCI-H460 cells at levels comparable to those observed in normal lung tissue, demonstrating that the expressed protein was wild-type p53. To explore whether wild-type p53 is a regulator in CT-1042-induced apoptosis, we assessed the expression of the p53 protein and its associated downstream proteins via western blotting. After treatment with various concentrations of CT-1042, the Bcl-2 expression decreased, whereas the Bax expression increased. Notably, the p53 protein was not detected or minutely detected in NCI-H460 cells. However, it significantly increased after drug treatment (Fig. 4B). Furthermore, we continued to detect the protein expression of STAT1, CYCS, Apaf-1, pro caspase-9 and survivin, as displayed in Fig. 4B. CT-1042 treatment resulted in a dose-dependent increase in the protein levels of STAT1, CYCS, Apaf-1 and pro-caspase-9 and a decrease in the protein level of survivin. These results indicated that the activation of the p53 protein is an initiating effector that promotes cellular apoptosis. Subsequently, the corresponding protein molecules
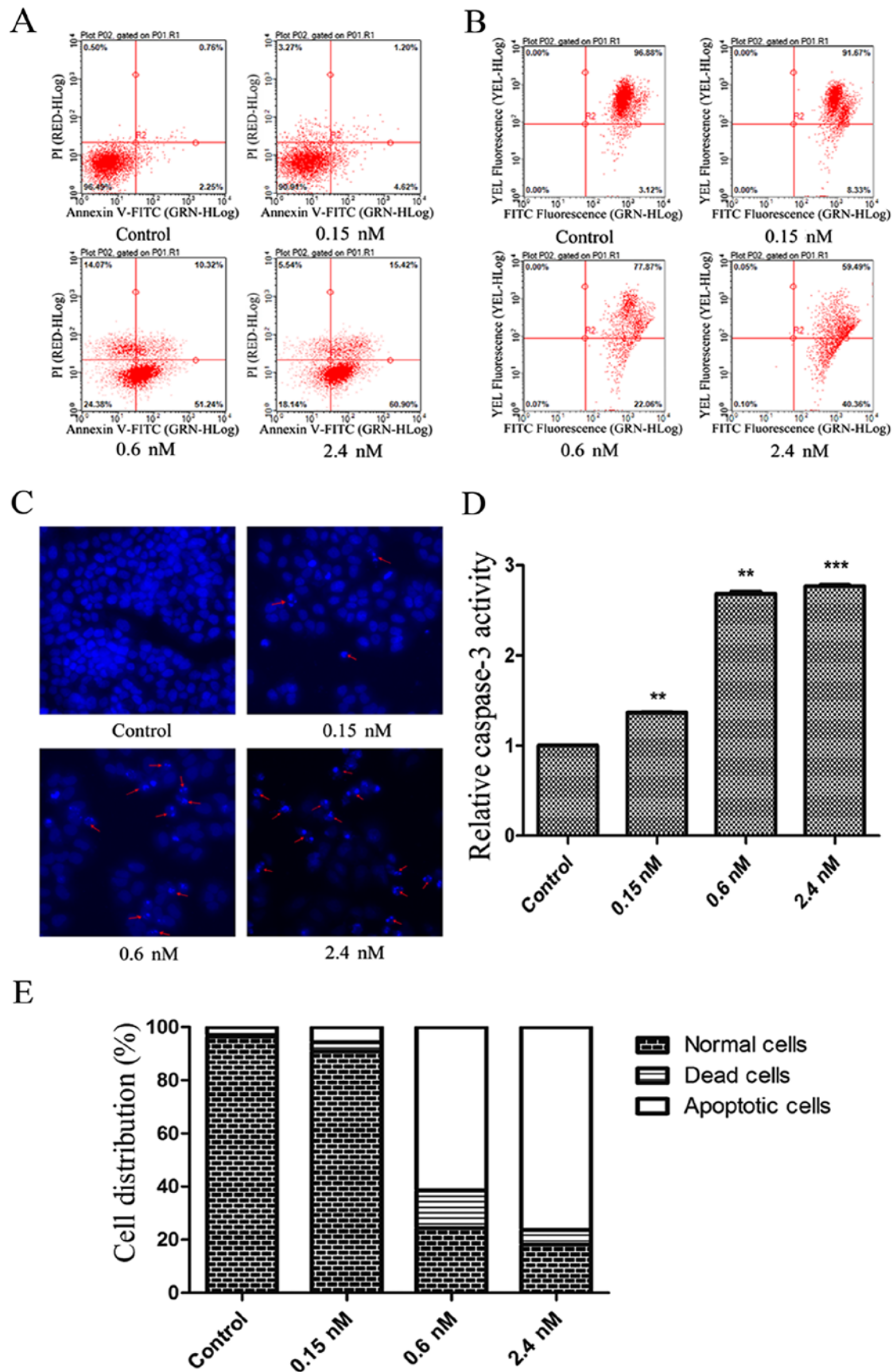
Figure 2. CT-1042 induces NCI-H460 cellular apoptosis. (A) NCI-H460 cells were treated with different concentrations of CT-1042 for 24 h, then stained with Annexin V-fluorescein isothiocyanate/propidium iodide (FITC/PI) and assessed with flow cytometry (FCM). (B) NCI-H460 cells were treated with different concentrations of CT-1042 for 24 h, then stained with the JC-1 fluorescent probe and captured with FCM. (C) NCI-H460 cells were treated with different concentrations of CT-1042 for 24 h, then stained with Hoechst 33342 and observed under a fluorescent microscope. (D) NCI-H460 cells were treated with different concentrations of CT-1042 for 24 h, then relative caspase-3 activity was assessed. (E) A column chart of the cell state distribution. [**]$P<0.01$, [***]$P<0.001$, compared with the control group.
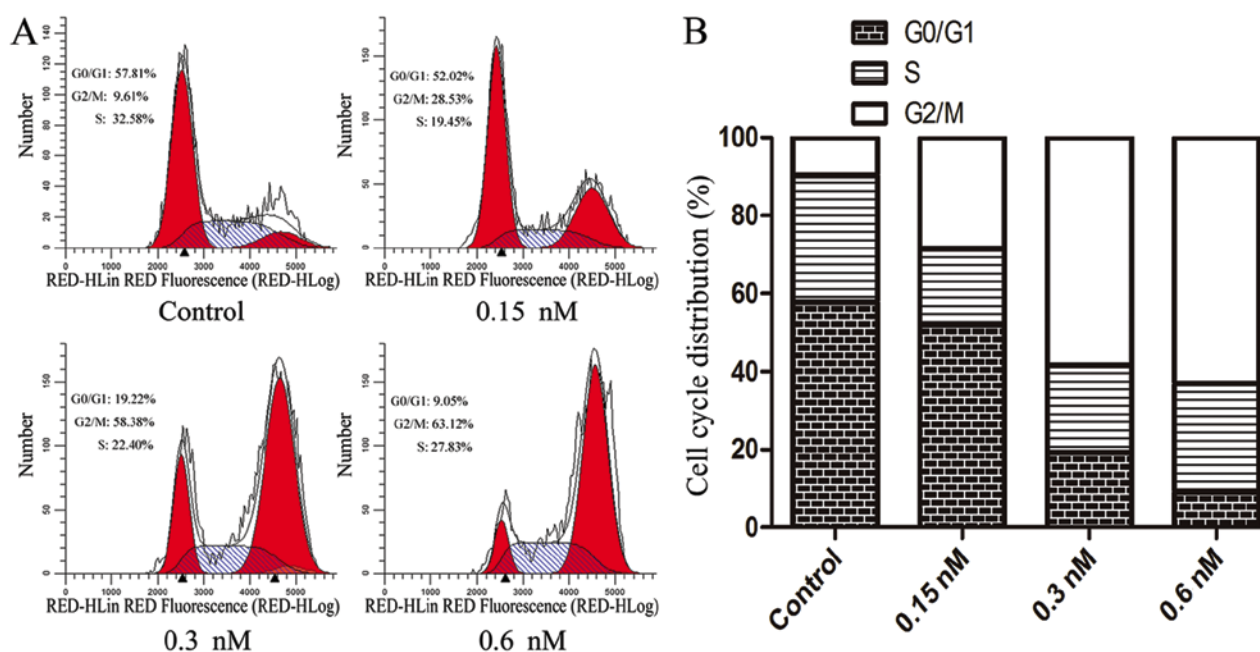
Figure 3. CT-1042 induces G2/M cell cycle arrest in NCI-H460 cells. (A) NCI-H460 cells were treated with CT-1042 (0, 0.15, 0.3 and 0.6 nM, respectively) for 24 h and analyzed for propidium iodide (PI)-stained DNA content using flow cytometry (FCM). (B) A column chart of the cell cycle distribution is shown.

Table III. Effect of CT-1042 on the growth of NCI-H460 xenograft tumor *in vivo*.

Groups	Route of administration	Number Start date	End date	Weight (mean ± SD) Start date	End date	Tumor volume (V, mm³)	Tumor weight (W, g)	Inhibition rate (%) V	W
Control	-	8	8	23.4±0.7	24.6±0.7	1219.2±791.2	1.100±0.706	-	-
Paclitaxel	i.v.x5	8	8	23.2±1.2	22.5±1.6[b]	168.2±110.1[b]	0.135±0.112[b]	86.2	87.8
High dose	i.v.x2	8	8	22.8±1.6	23.6±2.0	249.7±157.6[b]	0.217±0.119[b]	79.5	80.2
Middle dose	i.v.x2	8	8	23.4±2.5	24.0±3.3	387.2±310.8[a]	0.351±0.276[a]	68.2	68.0
Low dose	i.v.x2	8	8	23.3±1.1	24.4±1.2	417.5±355.1[a]	0.377±0.318[a]	65.8	65.7

[a]$P<0.05$, [b]$P<0.01$, compared with control group. V, volume; W, weight.

are activated or inhibited by the mitochondrial apoptosis pathway. Furthermore, expression of the proto-oncogenes c-met and c-myc was detected; we revealed that the protein expression of c-met and c-myc was reduced with increasing concentrations of CT-1042. PARP analysis demonstrated that the effects of CT-1042 on pro-PARP and cleaved-PARP were greater in NCI-H460 cells than in the control group (Fig. 4B).

Effect of CT-1042 on xenograft tumor growth in vivo. To evaluate whether CT-1042 inhibited tumor growth *in vivo*, NCI-H460 tumor pieces were injected into nude mice to establish a NCI-H460 subcutaneous tumor xenograft model. On day 15, mice were sacrificed, tumor xenografts were excised (Fig. 5A), and inhibition rate was calculated (Table III). The results indicated that CT-1042 induced a dose-dependent inhibition of NCI-H460 tumor volume and tumor weight, with an inhibition rate of tumor volume (V) of 79.5% and an inhibition rate of tumor weight (W) of 80.2% in the high-dose group. The middle- and low-dose groups also had significant effects (Fig. 5B and C). As displayed in Fig. 5D, all groups demonstrated an increase in body weight over time, however, body weights in the paclitaxel group slightly decreased.

In addition, H&E staining of tumor tissue from the control group did not exhibit any marked abnormalities, however, the high-treatment and the paclitaxel group indicated increases in nuclear fragmentation (Fig. 6). IHC results indicated strong Ki-67 and survivin staining and weak cleaved caspase-3 staining in the control group, whereas the test group and paclitaxel group exhibited weak Ki-67 and survivin staining and strong cleaved caspase-3 staining (Fig. 6). These results indicated that CT-1042 was effective at inhibiting xenograft tumor growth *in vivo* maybe by inhibiting tumor cell proliferation and promoting apoptosis.
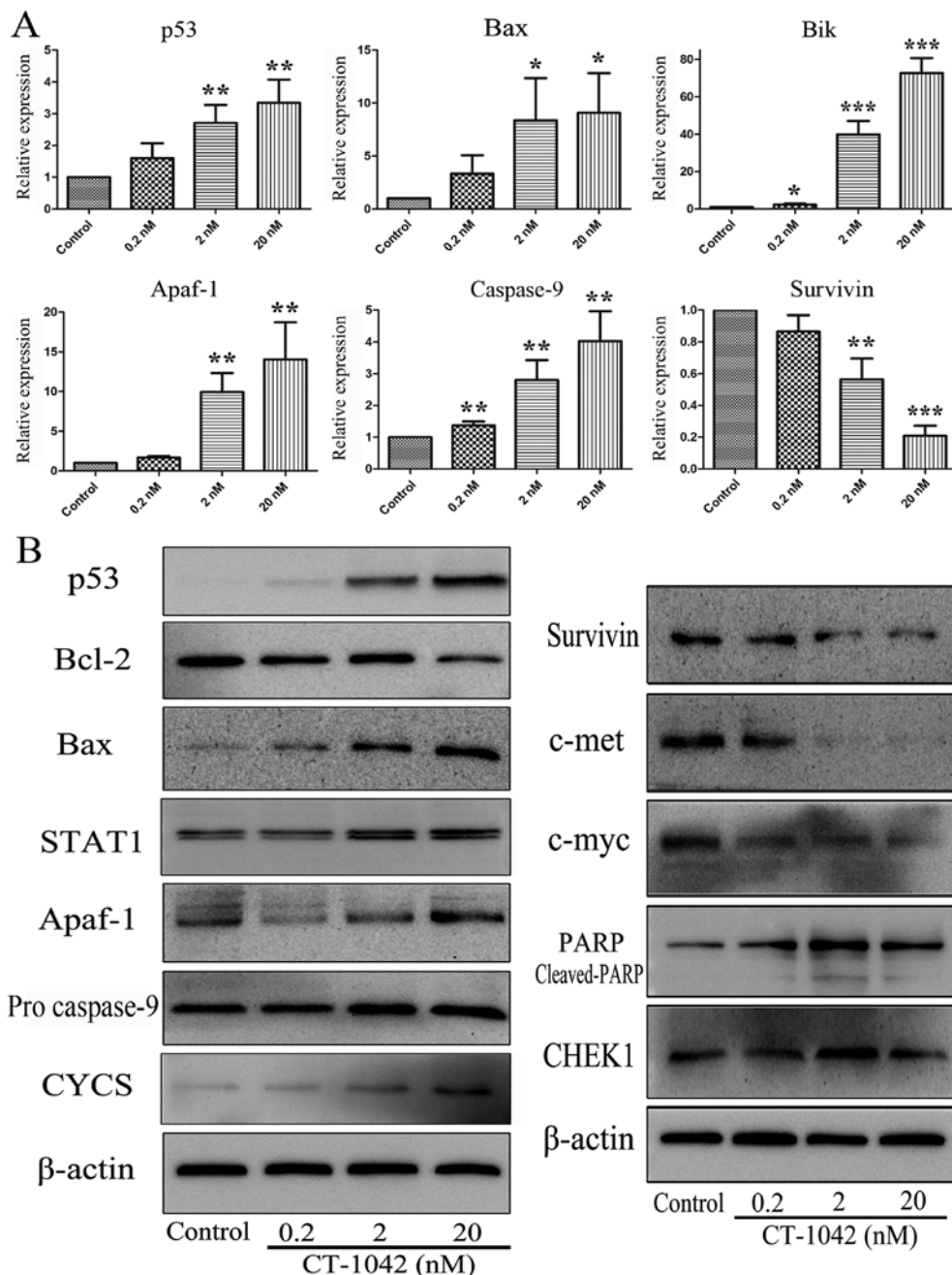
Figure 4. Effects of CT-1042 on the activation of p53 and mitochondria-mediated apoptosis in NCI-H460 cells. (A) Total RNA was extracted from treated and non-treated tumor cell samples and the transcriptome levels of *p53*, *Bax*, *Bik*, *Apaf-1*, *caspase-9* and *survivin* were quantified using qPCR. (B) Cells were treated with CT-1042 at 0 (control), 2 or 20 nM for 24 h, then total proteins were collected and analyzed via western blotting as described in Materials and methods. β-actin was used as a loading control. The results are representative of two independent experiments. *P<0.05, **P<0.01 and ***P<0.001, compared with the control group.

Discussion

Cancer cells are genetically unstable, therefore, it is easy to initiate apoptosis. Despite this instability of the genome, tumor cells can survive and continue to divide and proliferate, which is attributable to a strong anti-apoptotic mechanism in tumor cells (23). The relationship between anti-apoptotic proteins, such as Bcl-2 and survivin, as well as pro-apoptotic proteins, such as p53 and Bax, plays an important role. Specifically, Bcl-2 and survivin are highly expressed in most tumor cells, whereas p53 and Bax are marginally expressed proteins. An imbalance between pro- and anti-apoptotic proteins leads to

the emergence of tumor cell resistance to apoptosis. Therefore, regaining this balance and inducing apoptosis are considered effective therapeutic strategies against cancer progression. The small-molecule compound in this study, CT-1042, reverses this imbalance and induces apoptosis in tumor cells, exerting high anticancer activity.

In the present study, we demonstrated that CT-1042 effectively inhibited the proliferation of NCI-H460 NSCLC cells with an IC_{50} value of 0.166 nmol/l. Furthermore, Annexin V and PI double staining and the MMP assay both demonstrated the occurrence of cell apoptosis after CT-1042 treatment. These results were confirmed via Hoechst 33342 staining,
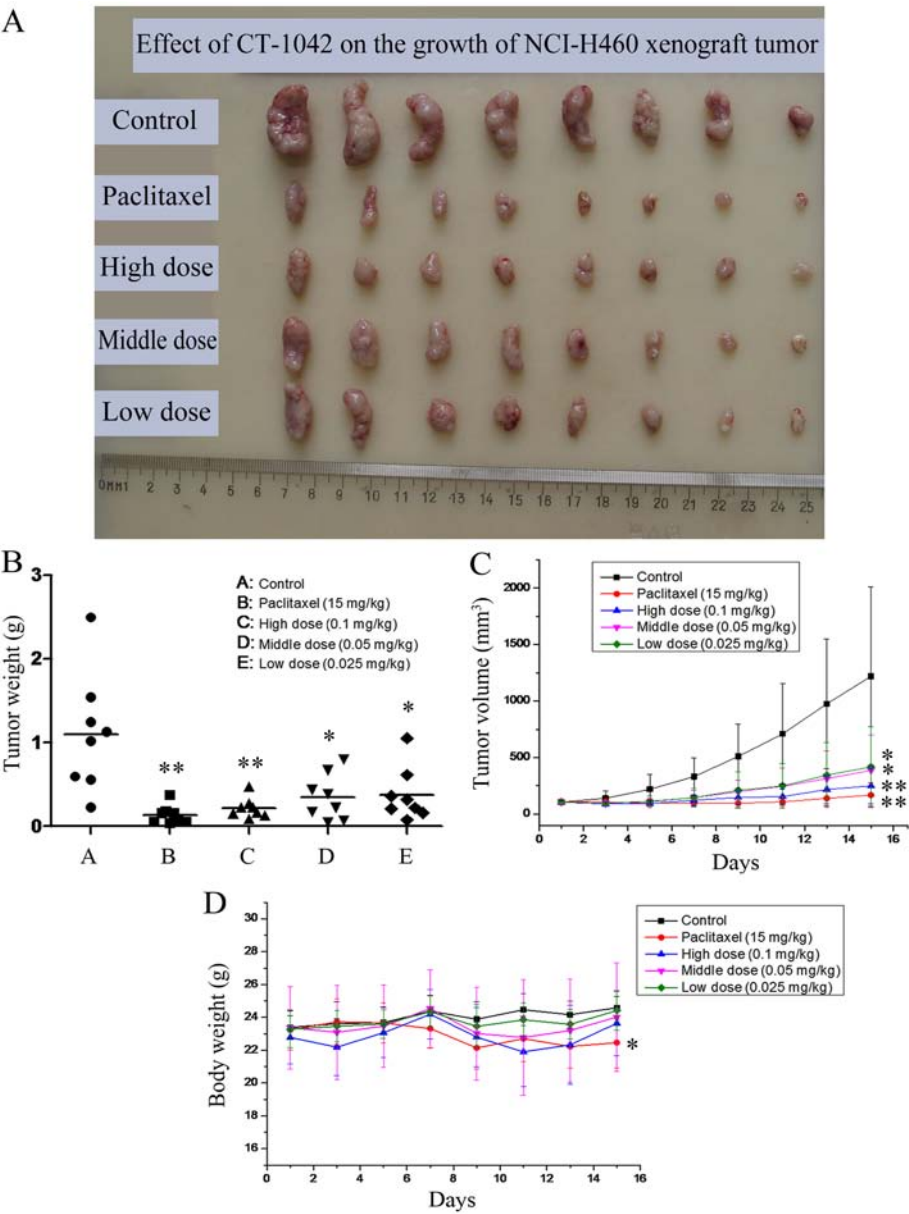
Figure 5. Effects of CT-1042 on the growth of NCI-H460 xenograft tumors *in vivo*. (A) Mice were treated with paclitaxel or CT-1042 and tumors were excised from the animals following treatment. (B) Tumor mass weights are shown. (C) Tumor volumes, assessed and calculated once every 2 days, are shown. (D) Body weights are shown. *P<0.05, **P<0.01, compared with the control group.
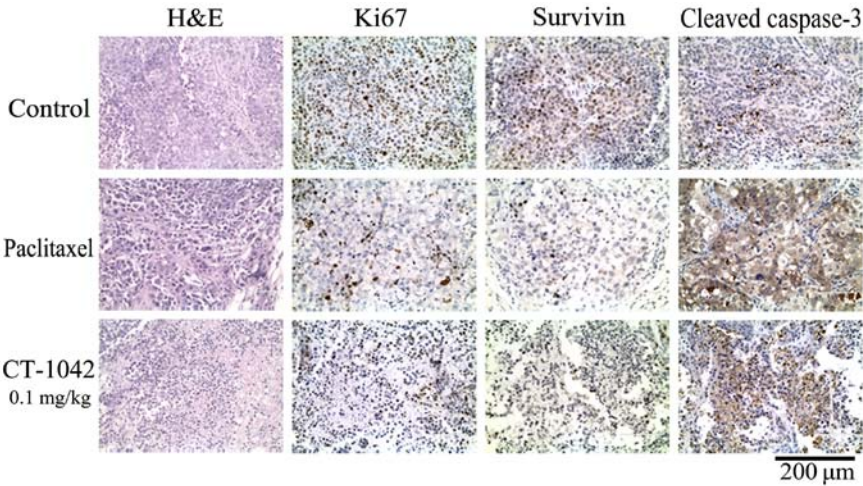

Figure 6. Hematoxylin and eosin (H&E) staining, along with detection of Ki-67, survivin, and cleaved caspase-3 expression in tumor xenograft tissues via immunohistochemistry.

which allowed us to determine the nuclear morphology. Dysregulation of the cell cycle is a key feature of tumor cells, thus targeting the cell cycle is an important strategy in cancer therapy. Cell cycle arrest is the main pathway involved in inhibiting tumor cell proliferation (24-26). Furthermore, the activation of cell cycle checkpoints is a general cell response following exposure to cytotoxic agents (27,28). In the present study, we revealed that CT-1042 arrested NCI-H460 cell cycle progression in the G2/M phase with increasing concentrations.

Two pathways of apoptosis have been identified: i) the death receptor pathway, which is initiated by the ligand-induced activation of death receptors; and ii) the mitochondrial pathway, which is triggered via numerous stress signals, including damage to cellular DNA. The mitochondrial pathway is primarily maintained by balancing the expression of pro-apoptotic and anti-apoptotic proteins of the Bcl-2 family (29,30). The expression of p53 was significantly enhanced following the administration of CT-1042, as demonstrated by western blot analysis and RT-qPCR. Furthermore, the Bcl-2/Bax and caspase-9 signaling pathways were identified and Bcl-2 was reduced, whereas Bax, CYCS, Apaf-1 and pro-caspase-9 increased. These results indicated that CT-1042 induced apoptosis via the p53 activation, followed by Bax promotion and Bcl-2 suppression, which promoted the release of CYCS and enhanced the expression of Apaf-1 and pro-caspase-9. In addition, NCI-H460 cell apoptosis was induced via the activation of downstream caspase cascade. Conversely, survivin is the smallest member of the inhibitor of apoptosis family (IAP) and is involved in inhibiting apoptosis and regulating the cell cycle (31,32). The expression of survivin in tumors is known to inhibit apoptosis and decrease cell death. However, it is also associated with chemotherapy tolerance and tumor invasion. Research has demonstrated that both the mRNA and protein expression of survivin decrease, indicating that it is related to the increase in caspase-9 and expansion of the apoptosis signal. Furthermore, proto-oncogenes are associated with normal cells and their abnormal activation can promote tumorigenesis. CT-1042 inhibited the expression of c-met and c-myc in cells, which prevented the proliferation of tumor cells and destroyed tumor growth balance.

Change in body weight is an important index for the initial evaluation of drug safety (33). All animals in the *in vivo* tumor xenograft experiment survived, with no other abnormalities, including general behaviors and body weights throughout the 15-day study. These results demonstrated that CT-1042 significantly inhibited tumor growth, with the lower dose resulting in lower toxicity and a better safety index. H&E staining and IHC results also confirmed that tumor proliferation was weakened and that apoptosis occurred in the treatment group.

In conclusion, our findings revealed that the effects of CT-1042 on the growth of NCI-H460 cells were associated with increased p53 expression and restoration of the balance between anti- and pro-apoptotic proteins, leading to mitochondria-mediated apoptosis. These results offer a basis for further development of CT-1042 as a highly potent anticancer drug.

Availability of data and materials

The datasets used during the present study are available from the corresponding author upon reasonable request.

Authors' contributions

SY conceived and designed the study. JY, SW and DY performed the experiments. JY wrote the manuscript. LL, CX and SY reviewed and edited the manuscript. All authors read and approved the manuscript and agree to be accountable for all aspects of the research in ensuring that the accuracy or integrity of any part of the work are appropriately investigated and resolved.

Ethics approval and consent to participate

All experimental protocols were approved by the Ethics Committee of the Academy of Military Medical Sciences (Beijing, China).

Consent for publication

Not applicable.

Competing interests

The authors declare that they have no conflicts of interest to declare.

References

1. Wall ME and Wani MC: Camptothecin and taxol: From discovery to clinic. J Ethnopharmacol 51: 239-254, 1996.
2. Giovanella BC, Hinz HR, Kozielski AJ, Stehlin JS Jr, Silber R and Potmesil M: Complete growth inhibition of human cancer xenografts in nude mice by treatment with 20-(*S*)-camptothecin. Cancer Res 51: 3052-3055, 1991.
3. Martino E, Della Volpe S, Terribile E, Benetti E, Sakaj M, Centamore A, Sala A and Collina S: The long story of camptothecin: from traditional medicine to drugs. Bioorg Med Chem Lett 27: 701-707, 2017.
4. Ryan JJ: Tyrosine kinase inhibitors in pulmonary vascular disease. JACC Basic Transl Sci 1: 684-686, 2016.
5. Rahman Jazieh A, Abdelhafiez N, Al Olayan A, Bamefleh H and Loutfi S: Tyrosine kinase inhibitors: What after complete remission of lung cancer? Cancer Treat Res Commun 11: 17-20, 2017.
6. Cayssials E and Guilhot F: Beyond tyrosine kinase inhibitors: Combinations and other agents. Best Pract Res Clin Haematol 29: 271-283, 2016.
7. Lin Z, Zhang Q and Luo W: Angiogenesis inhibitors as therapeutic agents in cancer: Challenges and future directions. Eur J Pharmacol 793: 76-81, 2016.
8. Wang Z, Dabrosin C, Yin X, Fuster MM, Arreola A, Rathmell WK, Generali D, Nagaraju GP, El-Rayes B, Ribatti D, *et al*: Broad targeting of angiogenesis for cancer prevention and therapy. Semin Cancer Biol 35 (Suppl): S224-S243, 2015.
9. Kise K, Kinugasa-Katayama Y and Takakura N: Tumor microenvironment for cancer stem cells. Adv Drug Deliv Rev 99: 197-205, 2016.

10. Umesalma S, Nagendraprabhu P and Sudhandiran G: Ellagic acid inhibits proliferation and induced apoptosis via the Akt signaling pathway in HCT-15 colon adenocarcinoma cells. Mol Cell Biochem 399: 303-313, 2015.

11. Tyagi A, Singh RP, Agarwal C and Agarwal R: Silibinin activates p53-caspase 2 pathway and causes caspase-mediated cleavage of Cip1/p21 in apoptosis induction in bladder transitional-cell papilloma RT4 cells: Evidence for a regulatory loop between p53 and caspase 2. Carcinogenesis 27: 2269-2280, 2006.

12. Chargari C, Leteur C, Angevin E, Bashir T, Schoentjes B, Arts J, Janicot M, Bourhis J and Deutsch E: Preclinical assessment of JNJ-26854165 (Serdemetan1), a novel tryptamine compound with radiosensitizing activity in vitro and in tumor xenografts. Cancer Lett 312: 209-218, 2011.

13. Wang H and Yan C: A small-molecule p53 activator induces apoptosis through inhibiting MDMX expression in breast cancer cells. Neoplasia 13: 611-619, 2011.

14. Hasanzadeh M, Shadjou N and de la Guardia M: Current advancement in immunosensing of p53 tumor suppressor protein based on nanomaterials: Analytical approach. TrAC Trends in Analyt Chem 89: 13-20, 2017.

15. Enoch T and Norbury C: Cellular responses to DNA damage: Cell-cycle checkpoints, apoptosis and the roles of p53 and ATM. Trends Biochem Sci 20: 426-430, 1995.

16. Lazo PA: Reverting p53 activation after recovery of cellular stress to resume with cell cycle progression. Cell Signal 33: 49-58, 2017.

17. Zeng L, Li T, Xu DC, Liu J, Mao G, Cui MZ, Fu X and Xu X: Death receptor 6 induces apoptosis not through type I or type II pathways, but via a unique mitochondria-dependent pathway by interacting with Bax protein. J Biol Chem 287: 29125-29133, 2012.

18. Ha M, Wei L, Guan X, Li L and Liu C: p53-dependent apoptosis contributes to di-(2-ethylhexyl) phthalate-induced hepatotoxicity. Environ Pollut 208: 416-425, 2016.

19. Gao CF, Ren S, Zhang L, Nakajima T, Ichinose S, Hara T, Koike K and Tsuchida N: Caspase-dependent cytosolic release of cytochrome *c* and membrane translocation of bax in p53-induced apoptosis. Exp Cell Res 265: 145-151, 2001.

20. Feng JH: Establishment of a cell strain from human kidney cell carcinoma KCC-853. Zhonghua Bing Li Xue Za Zhi 17: 102-104, 1988 (In Chinese).

21. Livak KJ and Schmittgen TD: Analysis of relative gene expression data using real-time quantitative PCR and the $2^{-\Delta\Delta C_T}$ method. Methods 25: 402-408, 2001.

22. Lopez J and Tait SW: Mitochondrial apoptosis: killing cancer using the enemy within. Br J Cancer 112: 957-962, 2015.

23. Yuan H, Cao Y, Li L, Wang S, Yang D, Zhong X, Tang S and Yuan S: SM-1 induces apoptosis of BGC-823 cells by activating procaspase-3 and exerts antitumor effect. Mil Med Sci 40: 326-330, 2016.

24. Barre B and Perkins ND: A cell cycle regulatory network controlling NF-kappaB subunit activity and function. EMBO J 26: 4841-4855, 2007.

25. Fu Y, Kadioglu O, Wiench B, Wei Z, Gao C, Luo M, Gu C, Zu Y and Efferth T: Cell cycle arrest and induction of apoptosis by cajanin stilbene acid from *Cajanus cajan* in breast cancer cells. Phytomedicine 22: 462-468, 2015.

26. Li Y, Yang F, Zheng W, Hu M, Wang J, Ma S, Deng Y, Luo Y, Ye T and Yin W: *Punica granatum* (pomegranate) leaves extract induces apoptosis through mitochondrial intrinsic pathway and inhibits migration and invasion in non-small cell lung cancer in vitro. Biomed Pharmacother 80: 227-235, 2016.

27. Pasetto LM, D'Andrea MR, Brandes AA, Rossi E and Monfardini S: The development of platinum compounds and their possible combination. Crit Rev Oncol Hematol 60: 59-75, 2006.

28. Voland C, Bord A, Peleraux A, Penarier G, Carriere D, Galiegue S, Cvitkovic E, Jbilo O and Casellas P: Repression of cell cycle-related proteins by oxaliplatin but not cisplatin in human colon cancer cells. Mol Cancer Ther 5: 2149-2157, 2006.

29. Saralamma VV, Nagappan A, Hong GE, Lee HJ, Yumnam S, Raha S, Heo JD, Lee SJ, Lee WS, Kim EH and Kim GS: Poncirin induces apoptosis in AGS human gastric cancer cells through extrinsic apoptotic pathway by up-regulation of Fas ligand. Int J Mol Sci 16: 22676-22691, 2015.

30. Kee JY, Han YH, Kim DS, Mun JG, Park J, Jeong MY, Um JY and Hong SH: Inhibitory effect of quercetin on colorectal lung metastasis through inducing apoptosis, and suppression of metastatic ability. Phytomedicine 23: 1680-1690, 2016.

31. Garg H, Suri P, Gupta JC, Talwar GP and Dubey S: Survivin: A unique target for tumor therapy. Cancer Cell Int 16: 49, 2016.

32. Altieri DC: Survivin-the inconvenient IAP. Semin Cell Dev Biol 39: 91-96, 2015.

33. Zhang C, Wang W, Liu T, Wu Y, Guo H, Wang P, Tian Q, Wang Y and Yuan Z: Doxorubicin-loaded glycyrrhetinic acid-modified alginate nanoparticles for liver tumor chemotherapy. Biomaterials 33: 2187-2196, 2012.